Switching Liquid Morphologies on Linear Grooves

Article *in* Langmuir · January 2008

DOI: 10.1021/la701899u · Source: PubMed

Switching Liquid Morphologies on Linear Grooves

Krishnacharya Khare,[†] Stephan Herminghaus,[†] Jean-Christophe Baret,[‡] Bruce M. Law,[§] Martin Brinkmann,[†] and Ralf Seemann*,[†]

Max Planck Institute for Dynamics and Self-Organization, D-37018 Göttingen, Germany, ISIS-ULP, BP 70028, 67083 Strasbourg Cedex, France, and Department of Physics, Kansas State University, Manhattan, Kansas 66506

Received June 26, 2007. In Final Form: August 10, 2007

The morphology of liquids confined to linear micrometer-sized grooves of triangular and rectangular cross section is studied for different substrate wettabilities. Depending on the wettability and exact geometry, either droplike morphologies or elongated liquid filaments represent the generic equilibrium structures on the substrate. Upon changing the apparent contact angle of aqueous drops by electrowetting, we are able to trigger the transition between elongated filaments and droplets. In the case of rectangular grooves, this transition allows us to advance liquid reversibly into the grooves while crossing a certain threshold contact angle. In triangular grooves, however, these elongated filaments undergo a dynamic instability when the contact angle returns to a value above the filling threshold. The different filling and drainage behavior is explained by specific aspects of the triangular and rectangular groove geometry.

1. Introduction

Generally, there are two strategies to guide liquids by open microfluidic structures. The first one is to prepare patterns with different wettability on planar substrates, which can be either static[1−6] or active (e.g., through electrowetting on patterned electrodes[7,8] or using temperature gradients[1,9,10]). A major disadvantage of this approach is that the Laplace pressure of any equilibrium liquid morphology in contact with a planar surface must be strictly positive, and a liquid will never spread spontaneously along the chemical patterns when brought into contact with a liquid reservoir at small Laplace pressure.

The second strategy is to offer an appropriate surface topography to the liquid.[11−13] This exploits the fact that the liquid wets the wedges and grooves rather than planar surfaces, provided that the contact angle with the substrate material is sufficiently small. Depending on control parameters such as contact angle, liquid volume, and the geometry of the surface topography, a rich variety of liquid morphologies can be found at steps[12] and in rectangular grooves.[13]

For large contact angles, the liquid will form dropletlike morphologies on a grooved substrate regardless of the underlying topography. If the contact angle falls below a threshold value, which depends on the particular geometry of the groove, the liquid invades the groove and forms elongated filaments. These liquid filaments can have either positive or negative Laplace pressure,[14,15] which allows the filling of the grooves if the liquid is in contact with a reservoir at zero pressure.[16−21] Combined with a technique to vary the wettability, it can be utilized to transport liquids on demand along grooves.[13,22,23]

In this article, we study the spectrum of liquid structures in contact with linear grooves of different cross sections, both experimentally and theoretically. The liquid morphologies in triangular grooves are compared to those found on substrates with rectangular grooves. Using the electrowetting effect,[8,24−27] we were in both cases able to reduce the apparent contact angle of the liquid below the respective filling threshold. Then, a liquid filament advances into the groove from a large feeding drop, as we explicitly demonstrate. In contrast to rectangular grooves, where the filling is fully reversible,[13,22,23] liquid filaments in triangular grooves decay into isolated droplets once the contact angle is again increased above the filling threshold.[28] This peculiar behavior results from the specific geometry of a triangular groove and will also be discussed in comparison to rectangular grooves.

2. Experimental Section

Grooves with a triangular cross section were fabricated in silicon (Si) in a straightforward manner by standard photolithography with subsequent anisotropic wet etching. This procedure leads to an opening angle of $\alpha = 70.6°$ as determined by the crystal lattice of silicon (Figure 1). For convenience, we will mostly refer to the

* Corresponding author. E-mail: ralf.seemann@ds.mpg.de.
† Max Planck Institute for Dynamics and Self-Organization.
‡ ISIS-ULP.
§ Kansas State University.

(1) Darhuber, A. A.; Troian, S. M. *Annu. Rev. Fluid Mech.* **2005**, *37*, 425.
(2) Gau, H.; Herminghaus, S.; Lenz, P.; Lipowsky, R. *Science* **1999**, *283*, 46.
(3) Brinkmann, M.; Lipowsky, R. *J. Appl. Phys.* **2002**, *92*, 4296.
(4) Kataoka, D.; Troian, S. *Nature* **1999**, *402*, 794.
(5) Wang, J.; et al. *Nat. Mater.* **2004**, *3*, 171.
(6) Zhao, B.; et al. *Science* **2001**, *291*, 1023.
(7) Hayes, R. A.; Feenstra, B. J. *Nature*, **2003**, *425*, 383. Hayes, R. A.; Feenstra, B. J. *Annu. Rev. Fluid Mech.* **2005**, *37*, 425.
(8) Mugele, F.; Baret, J.-C. *J. Phys.: Condens. Matter* **2005**, *17*, R705.
(9) Daniel, S.; Chaudhury, M. K.; Chan, J. C. *Science* **2001**, *291*, 633.
(10) Darhuber, A. A.; Valentino, J. P.; Davis, J. M.; Troian, S. M.; Wagner, S. *Appl. Phys. Lett.* **2003**, *82*, 657.
(11) Rascón, C.; Parry, A. O. *Nature* **2000**, *407*, 986.
(12) Brinkmann, M.; Blossey, R. *Eur. Phys. J. E* **2004**, *14*, 79.
(13) Seemann, R.; Brinkmann, M.; Kramer, E. J.; Lange, F. F.; Lipowsky, R. *Proc. Natl. Acad. Sci. U.S.A.* **2005**, *102*, 1848.
(14) Concus, P.; Finn, R. *Proc. Nat. Acad. Sci. U.S.A.* **1969**, *63*, 292.
(15) Concus, P.; Finn, R. *Acta Math.* **1974**, *132*, 177.
(16) Rye, R. R.; Mann, J. A., Jr.; Yost, F. G. *Langmuir* **1996**, *12*, 555.
(17) Yost, F. G.; Rye, R. R.; Mann, J., Jr. A. *Acta Mater.* **1997**, *45*, 5537.
(18) Rye, R. R.; Yost, F. G.; O'Toole, E. J. *Langmuir* **1998**, *14*, 3937.
(19) Weislogel, M. M.; Lichter, S. *J. Fluid Mech.* **1998**, *373*, 349.
(20) Warren, P. B. *Phys. Rev. E* **2004**, *69*, 041601.
(21) Dussaud, A. D.; Adler, P. M.; Lips, A. *Langmuir* **2003**, *19*, 7341.
(22) Baret, J.-C.; Decré, M.; Herminghaus, S.; Seemann, R. *Langmuir* **2005**, *21*, 12218.
(23) Baret, J.-C.; Decré, M.; Herminghaus, S.; Seemann, R. *Langmuir* **2007**, *23*, 5200.
(24) Quilliet, C.; Berge, B. *Europhys. Lett.* **2002**, *60*, 99.
(25) Someya, T.; Dodabalapur, A.; Gelperin, A.; Katz, H. E.; Bao, Z. *Langmuir* **2002**, *18*, 5299.
(26) Prins, M. W.; Welters, W. J. J.; Weekamp, J. W. *Science* **2001**, *291*, 277.
(27) Lippmann, G. *Ann. Chim. Phys.* **1875**, *5 e* séries, t. V.
(28) Khare, K.; Brinkmann, M.; Law, B. M.; Gurevich, E.; Herminghaus, S.; Seemann, R. *Langmuir*, accepted for publication.

10.1021/la701899u CCC: $37.00
Published on Web 11/15/2007

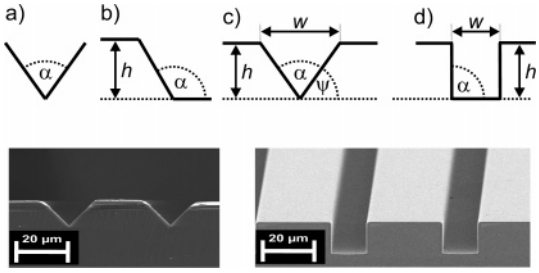

Figure 1. (Top) Sketch of various cross sections (from left to right): infinite wedge, topographic step, finite wedge, and rectangular groove geometry. The aspect ratio for a rectangular groove is defined as $X = h/w$. (Bottom) SEM micrographs of triangular and rectangular grooves in Si. Fixed by the substrate geometry, we have $\psi \simeq 54.7°$ for triangular grooves and $\psi \simeq 90°$ for rectangular grooves.

wedge angle $\psi = 90° - \alpha/2$ instead of the opening angle α. To fabricate grooves with a rectangular cross section, isotropic reactive ion etching had to be applied. In this way, grooves were fabricated over a range of aspect ratios, $X = 0.04-1.33$, defined as the ratio of groove height h to groove width w. The geometry and surface roughness of the grooves have been characterized by atomic force microscopy (AFM) and by scanning electron microscopy (SEM), as can be seen in Figure 1. Typically, the surface roughness was below 0.3 nm. The width of the grooves varied between 400 nm and 20 μm.

To create liquid morphologies, the substrates were exposed for 6−48 h to oversaturated vapor of short-chain polystyrene that condenses on the substrate. The polystyrene with a molecular weight of $M_w = 1.89$ and 2.25 kg/mol and a monodispersity of $M_w/M_n = 1.06$ was purchased from PSS (Mainz, Germany). Upon lowering the temperature below the glass-transition temperature of polystyrene, the liquid structures "freeze", and their shape could be imaged easily by AFM in tapping mode. The shape of the wetting morphology before and after freezing the polystyrene remains identical, as proven in previous studies.[29,30]

The contact angle θ that the polystyrene melt forms with the substrate was modified by hydrophobizing the silicon substrates with a self assembled monolayer (SAM). After a thorough cleaning using standard procedures,[34] a monolayer of semifluorinated trichlorosilane, $[F(C_2F)_8(CH_2)_2SiCl_3]$, was deposited from the vapor phase onto the silicon substrates. To fine tune the wettability of the coated substrates, a subsequent oxygen plasma treatment was performed. Thus, we could prepare contact angles for the polystyrene melt on the substrate ranging from $\theta = 5°$ to 80° which corresponds to the clean silicon substrate and the trichlorosilane monolayer, respectively.[13]

In general, one expects some contact angle hysteresis corresponding to the difference between advancing and receding contact angles. Because the liquid morphologies were formed by condensation, the measured contact angles are likely to represent advancing contact angles. As more liquid volume is condensed in a groove, the liquid structures merge and reorganize, which could also involve some receding parts. The small variance of the measured contact angle seems to indicate that the contact angle hysteresis was small.

3. Results and Discussion

3.1. Static Liquid Morphologies. To obtain a fundamental understanding of how edges and corners determine the wetting morphologies on a topographically structured surface, let us start

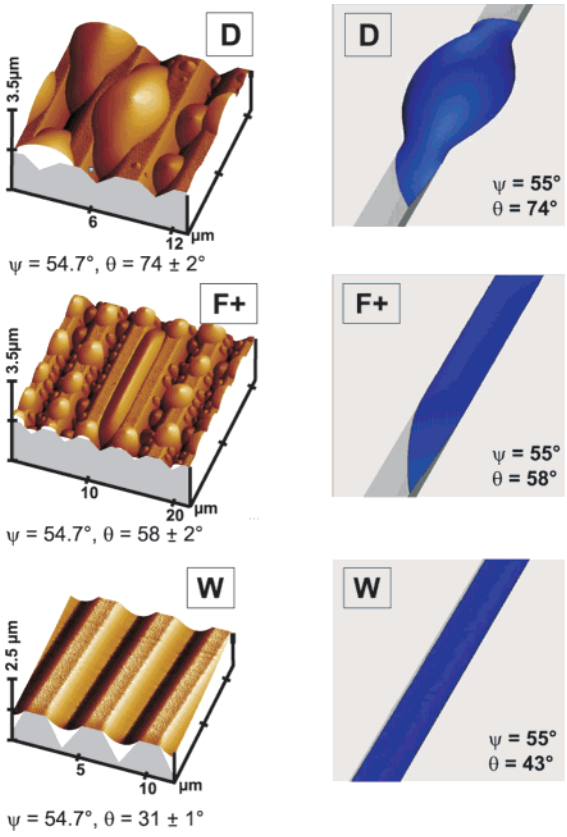

Figure 2. Liquid morphologies in grooves with triangular cross sections. AFM images of PS morphologies condensed from the vapor phase and numerical results are displayed in the left and right columns, respectively. Localized droplets (D) form at high contact angles, and extended filaments with positive Laplace pressure (F+) are found just above the filling angle $\theta = \psi$. Liquid wedges (W) with a concave meniscus emerge for contact angles of $\theta < \psi$.

our consideration with the simplest topography, an infinite wedge with opening angle α, and increase the complexity by adding corners and edges as sketched in Figure 1. In infinite wedges, the wetting liquid forms either droplike morphologies or liquid filaments extending along the entire length of the wedge, depending on whether the contact angle is larger or smaller than $90° - \alpha/2$. The only natural length scale in this scenario is set by the cube root of the droplet volume.

Another elementary geometry sketched in Figure 1 is a topographic step. The step height h introduces an additional length scale, which gives rise to qualitatively new liquid morphologies.[12] Provided that either the droplet volume or the contact angle θ is sufficiently small, the respective morphologies found in a finite wedge are identical to those of the respective infinite wedge. But, in contrast to infinite wedges, also elongated liquid morphologies of finite extension may appear at a topographic step.

The spectrum of liquid morphologies on triangular grooves at larger liquid volume is shown in Figure 2. It comprises localized droplets (D), elongated filaments (F), and liquid wedges (W). Dropletlike morphologies dominate for large contact angles θ. In this case, the liquid morphologies are not confined to the grooves and spread on top of the ridges. The liquid−vapor interface of a localized droplet is always curved to the vapor phase, which implies that the Laplace pressure of this morphology is positive.

For smaller contact angles, the liquid tries to follow the symmetry of the underlying substrate. The liquid is confined to the grooves forming filaments with a homogeneous cross section

(29) Seemann, R.; Herminghaus, S.; Jacobs, K. *J. Phys.: Condens. Matter* **2001**, *13*, 4925. Seemann, R.; Herminghaus, S.; Jacobs, K. *Phys. Rev. Lett.* **2001**, *87*, 196101.
(30) Seemann, R.; Jacobs, K.; Blossey, R. *J. Phys.: Condens. Matter* **2001**, *13*, 4925.
(31) Lipowsky, R.; Lenz, P.; Swain, P. S. *Colloids Surf., A* **2000**, *161*, 3.
(32) Young, T. *Philos. Trans. R. Soc.* **1805**, part I, 65.
(33) Brakke, K. *Exp. Math.* **1990**, *1*, 141. Brakke, K. *Exp. Math.* **2000**, *87*, 7768.
(34) Sagiv, J. *J. Am. Chem. Soc.* **1980**, *102*, 92.

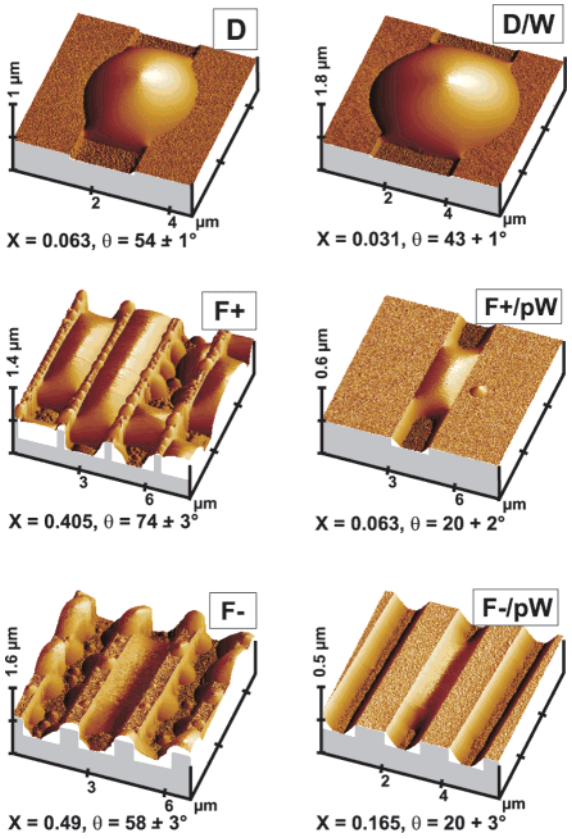

Figure 3. Liquid morphologies in rectangular grooves obtained by AFM. One observes overspilling droplets (D) that spread onto the ridges, extended filaments (F+) with positive Laplace pressure, and extended filaments (F−) with negative Laplace pressure. For a contact angle of $\theta < 45°$, one may find droplets (D) and filaments (F) that are connected to thin liquid wedges (W) in the groove corners.

of finite length. Besides the region close to both ends, the liquid−vapor interface of a filament is cylindrical and curved toward the vapor phase (F+). The contact line of the elongated filament is pinned to the upper edges of the grooves in its homogeneous parts. Only close to the terminal part of the meniscus does the contact line explore the plane walls of the groove.

At low contact angles, the liquid morphology spreads along the bottom of the groove, forming a homogeneous liquid wedge (W). Its liquid−vapor interface is again cylindrical but is curved toward the liquid phase. The contact lines of such a wedge is not pinned but resides on the side walls of the grooves at a height that is determined by the contact angle and the Laplace pressure.

Rectangular cross sections can be envisaged as being composed of two opposing steps of height h, both with a step angle of $\alpha = 90°$. For a large separation between these two steps, $w \gg h$, the groove can be regarded as two effectively independent steps that can be wetted by two independent liquid morphologies. When the separation, w, is reduced, the two rectangular wedges will finally interact via the liquid filament attached to them. When w is on the order of the step height, h, it is likely that liquid morphologies with a single meniscus appear, which are pinned to both upper edges of the steps. Hence, the second bottom corner permits the existence of wetting morphologies with one or two liquid menisci or even the coexistence of both types of morphologies in the same groove. As shown in Figure 3, the variety of equilibrium morphologies in rectangular grooves is clearly larger than the liquid morphologies found in triangular grooves. For instance, liquid morphologies with two disjointed menisci may occur in rectangular grooves.[13]

Similar to triangular grooves, two dominant liquid morphologies are found for a wide range of contact angles θ and aspect ratio $X = h/w$ in rectangular grooves: localized, dropletlike shapes (D) and elongated liquid filaments (F). Localized droplets (D) appear exclusively on samples with small aspect ratios or large contact angles. For smaller contact angles or larger aspect ratios, the liquid forms elongated filaments (F) with a cylindrical liquid−vapor interface being pinned to the edges of the groove. In contrast to triangular grooves, the liquid−vapor interface can be curved either toward the liquid or toward the vapor phase. For shallow grooves and large contact angles, we find filaments with positive Laplace pressure (F+) whereas filaments with negative Laplace pressure (F−) are encountered in deep grooves and for small contact angles. The length of such a liquid filament depends on the amount of liquid adsorbed to the groove. As for the triangular grooves, we observe that their cross section is homogeneous and independent of the filament length.

Below a certain contact angle, a second morphology class appears in combination with localized droplets and elongated filaments: the respective liquid morphology may continue as fine liquid wedges (W) wetting the corners of the groove on either side of the droplet or filament[13] (Figure 3).

3.2. Analytical Approximation. On a micrometer length scale, the equilibrium shape of an incompressible nonvolatile liquid is governed predominantly by its interfacial free energy. Corrections due to the long-range interaction between the liquid−solid and the liquid−vapor interfaces become relevant in the range of distances smaller than ~100 nm.[31] Gravitational effects, however, can be safely neglected if the extension of the liquid structures into the vertical direction is well below the capillary length, $l_{cap} = \sqrt{\gamma_{lv}/g|\Delta\rho|}$, where γ_{lv} is the interfacial tension of the liquid−vapor interface, $\Delta\rho = \rho_l - \rho_v$ is the density difference between the liquid (l) and vapor (v) phases, and g the gravitational acceleration. In our evaporation experiments, $l_{cap} \approx 1.7$ mm. Because the transverse dimension, L, of the surface topographies in our experiments (i.e., the width and depth of the grooves) is in the micrometer range, it is justified to apply the interfacial model here. An equivalent measure is the Bond number, $Bo = L^2/l_{cap}^2$, which is below $\sim 10^{-6}$ in our system. In what follows, a scheme is put forward that allows to predict the emerging wetting morphologies by means of an effectively 2D interface model.

On the relevant length scales of our experiments, the mean curvature of the liquid−vapor interface is constant at mechanical equilibrium. This follows directly from the Laplace equation, $\Delta P = 2H\gamma_{lv}$, that relates the difference $\Delta P = P_l - P_v$ between the pressure inside the liquid, P_l, and the vapor, P_v, to the interfacial tension, γ_{lv}, and the mean curvature, H, of the interface.[39]

The second equilibrium condition concerns the contact angle of the liquid with the substrate, θ. This condition is expressed by the Young−Dupré equation $\gamma_{lv} \cos\theta = \gamma_{sv} - \gamma_{sl}$, where γ_{sv} and γ_{sl} are the interfacial energies of the solid−vapor and solid−liquid interfaces, respectively.[32] The contact angle of a liquid is well defined by the Young−Dupré equation on smooth parts of the substrate; however, it becomes ill-defined whenever the contact line coincides with an acute kink of the substrate topography. In this case, the liquid−vapor interface is free, within the range of $\alpha - 180°$, to form any angle between the contact

(35) Matrick, R. F. *Transmission Lines for Digital and Commumication Networks*; McGraw-Hill: New York, 1969.
(36) Shuttleworth, R.; Bailey, G. L. J. *Discuss. Faraday Soc.* **1948**, *3*, 16.
(37) Buehrle, J.; Herminghaus, S.; Mugele, F. *Phys. Rev. Lett.* **2003**, *91*, 086101.
(38) Mugele, F.; Buehrle, J. *J. Phys.: Condens. Matter* **2007**, *19*, 375112.
(39) The mean curvature H is the sum, divided by 2, of two normal curvatures C_1 and C_2 along mutually orthogonal directions.

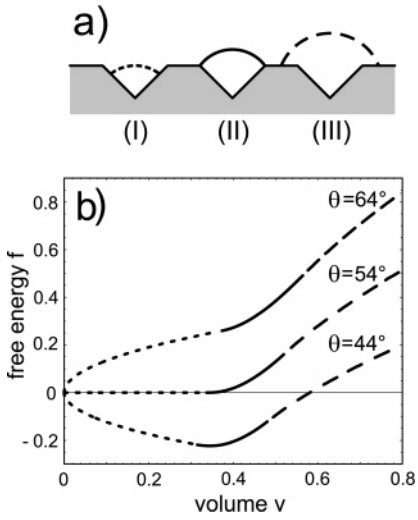

Figure 4. (a) Cross sections of possible homogeneous liquid morphologies in triangular grooves. Note that the curvature of all morphologies can be either positive or negative, except for morphology (III). (b) Rescaled free energy (1) of the shown liquid morphologies as a function of the rescaled volume v for a wedge angle of $\psi = 54°$. The dotted, solid, and dashed segments correspond to liquid contours (I−III), respectively, as shown in part a.

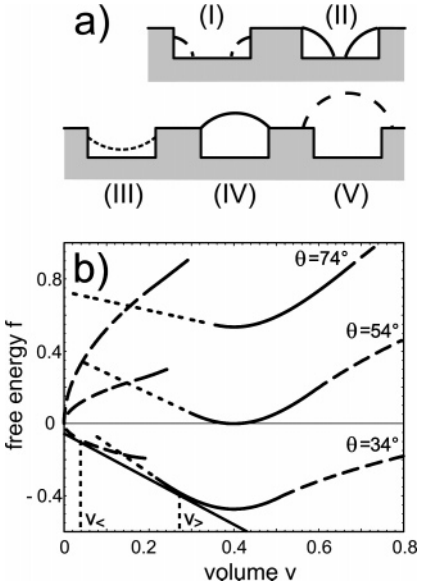

Figure 5. (a) Cross sections of possible homogeneous liquid morphologies in rectangular grooves. The curvature of all morphologies can be either positive or negative, except for morphology (V). (b) Rescaled free energy (1) of the shown liquid morphologies as a function of the rescaled volume v for a groove with an aspect ratio of $X = 0.5$. The line style corresponds to liquid contours I−IV shown in part (a).

angles with respect to either side of the kink.[40] Acute kinks immobilize the contact line as long as the contact angle falls into this free range. This effect is known as contact line pinning and represents a generic feature of liquid morphologies in contact with substrate topographies.[12,13]

On linear surface topographies, contact line pinning may lead to the formation of liquid morphologies with a homogeneous cross section. Beside regions close to the terminal part of the meniscus, their liquid−vapor interface is approximated by a cylindrical segment or a plane. This applies to elongated filaments (F) or liquid wedges (W) found in grooves of triangular cross section. For this particular groove geometry, one may construct three different types (I−III) of homogeneous morphologies, as illustrated in Figure 4a. The interfacial free energy per unit length of a homogeneous segment, f, can be computed from the contour lengths l_{lv} and l_{sl} of the liquid−vapor and the solid−liquid interfaces, respectively, as

$$f = \gamma_{lv}(l_{lv} - l_{sl}\cos\theta) \qquad (1)$$

The interfacial free energy of homogeneous liquid morphologies on triangular grooves is shown in Figure 4b for three different contact angles as a function of the liquid volume v (normalized by the groove length) for a fixed wedge angle $\psi \simeq 54.7°$. In general, the Laplace pressure of a homogeneous morphology corresponds to the slope $f'(v)$ of the free-energy curves. A homogeneous morphology will become unstable with respect to a longitudinal exchange of liquid if the second derivative $f''(v)$ is negative. This applies to the droplet morphology (III) and, for a contact angle of $\psi < \theta$, to morphology (I) (Figure 4b). Any variation in the liquid distribution will then be amplified because liquid is driven from regions of lower filling corresponding to a larger Laplace pressure toward regions of larger filling corresponding to a lower Laplace pressure.[28] In the course of such an instability, the liquid will decay into localized droplets (D) with a heterogeneous cross section.

(40) More precisely, if ϑ is the angle that the liquid makes with some plane of reference and x is the position of the contact line, then $dx/d\vartheta$ is given by the radius of curvature of the kink. For an acute kink, this is zero, corresponding to perfect pinning.

Liquid filaments (F) in triangular grooves can be described by a homogeneous configuration of type (II) in coexistence with a completely dewetted part of the groove. The range of liquid volume where the morphology (F) exists is limited by the length of the grooves. These filaments have a positive mean curvature throughout. Liquid wedges (W) with a negative Laplace pressure correspond to type (I) for contact angles of $\theta < \psi$. In contrast to filaments, liquid wedges extend over the entire length of the grooves. Accordingly, their cross section depends on the total volume per length of the groove. Liquid filaments (F) are metastable with respect to droplet morphology (D) if the liquid volume is large compared to the cube of the transverse dimensions of the groove.

For rectangular grooves, we restrict our analysis to liquid morphologies being symmetric with respect to the cross section of the groove. Five different homogeneous morphologies (I−V) at contact angles of $\theta < 90°$ are found, as displayed in Figure 5a. Examples of the corresponding interfacial free energy (1) of liquid morphologies in rectangular grooves with an aspect ratio of $X = 0.5$ are shown in Figure 5b for three different contact angles as a function of the liquid volume v. Generically, two branches of homogeneous morphology exist in the rectangular geometry: a branch at low volumes with two separate menisci (I−II), corresponding to the morphologies at a single step, and a second branch (III−V) at higher volumes with only one meniscus.

In a certain range of liquid volumes, piecewise homogeneous morphologies may occur as the state of lowest free energy.[13] In this case, the liquid may separate into two homogeneous segments at the same Laplace pressure. As the total amount of liquid in the groove is increased or decreased, one observes a gradual change in the length of a segment while its cross sections remain constant. The length of the crossover between two homogeneous parts is typically on the order of the channel width. The respective heterogeneous morphologies are constructed from the free energy (1) as a function of the volume per length, v, using the common tangent method, as we will discuss in the following paragraph for the particular values $X = 0.5$ and $\theta = 34°$.[12,13]

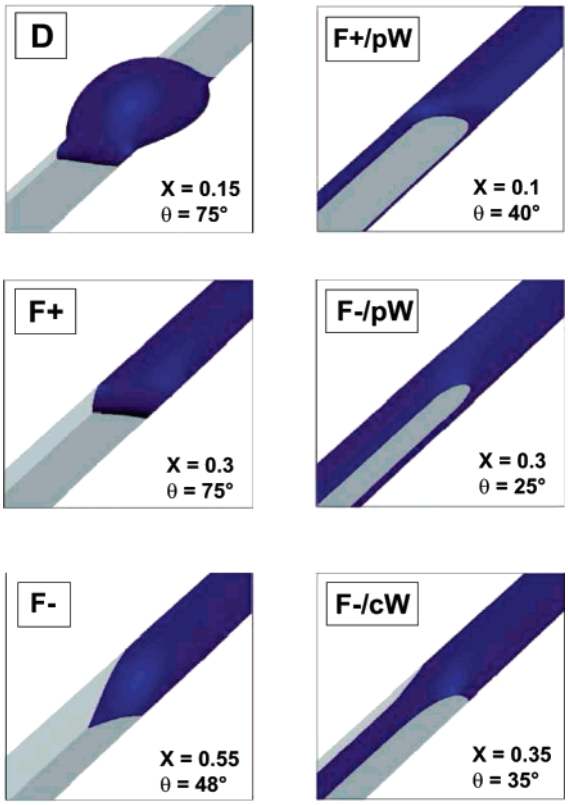

Figure 6. Liquid morphologies in rectangular grooves obtained from numerical minimizations of the interfacial energy. The same morphologies are found as in the AFM experiments (Figure 3).

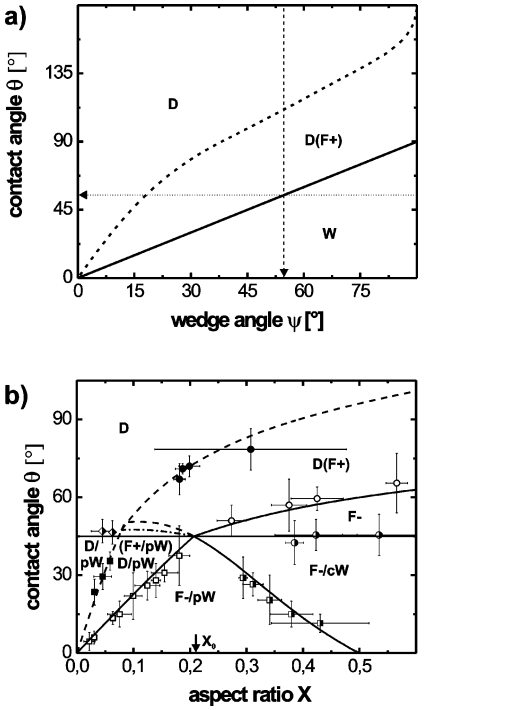

Figure 7. Morphology diagram of liquid confined to (a) triangular grooves and (b) rectangular grooves in the asymptotic limit of large volumes $V \gg w^3$. The data points in part (b) indicate the experimentally determined boundaries. Brackets denote metastable morphologies; coexistence is indicated by a slash between the respective morphologies.

In the range of low liquid volume, $v < v_<$, the liquid will be found in a symmetric homogeneous morphology of type (I), forming wedges in the bottom corners (cW). If v falls into the interval between $v_<$ and $v_>$, then the global minimum of the interfacial energy is a combination of the morphologies of type (I) at a volume of $v = v_<$ and (IV) at $v = v_>$; see also Figure 5. This piecewise homogeneous morphology can be identified with a filament (F−) at negative Laplace pressure continuing as liquid corner wedges (cW) wetting the remaining part of the groove.

To cross check our analytical model, we used numerical minimizations of the interfacial energy to detect locally and globally stable liquid shapes in the grooves. Throughout our investigations, we used the freely available software Surface Evolver.[33] In addition, the numerical minimizations allowed us to investigate the stability range of liquid morphologies whose curvature in the direction of the grooves is non-negligible. In particular, the numerical minimizations provide the means to investigate heterogeneous morphologies (D) as well as "short" filaments (F). It turns out that the 2D model is still valid regarding filaments with lengths roughly four times the channel width. The numerically obtained morphologies in the geometry of triangular grooves are displayed in the right column of Figure 2. As expected, we find morphologies consisting of two homogeneous parts in channels with rectangular cross sections. Figure 6 shows the numerical results in rectangular grooves for various aspect ratios and contact angles, including the heterogeneous morphology (D).

3.3. Morphology Diagrams. The appearance of different droplet morphologies is best illustrated in the form of a morphology diagram. In short, it displays regions of relevant control parameters where certain equilibrium liquid shapes exist as locally or globally stable shapes. The morphology diagrams presented in Figure 7 summarize all information about wetting morphologies in grooves with triangular and rectangular cross sections and provide a convenient way to compare the morphologies found in experiment and theory.

A cross section through any liquid morphology in a triangular groove exhibits a single meniscus. The morphology (F+) found at intermediate contact angles, θ, respectively, wedge angles, ψ, is metastable with respect to localized droplets (D), which is the generic morphology at large contact angles and small wedge angles. The dashed line in Figure 7a denotes the largest contact angle for a given wedge angle for which filaments with positive Laplace pressure can exist as locally stable shapes. The inverse transition (i.e., the decay of a droplet (D) into a filament (F+)) occurs close to the solid line in Figure 7a, where the Laplace pressure of the filament changes sign. In the asymptotic limit $V \gg w^3$, that we consider here, the line of instability falls onto the solid line representing filaments with zero Laplace pressure, and the transitions is simply given by $\theta = \psi$. In the regime below the solid line, liquid can be spontaneously drawn into the triangular grooves from a large feeding droplet forming liquid wedges (W) with a negative Laplace pressure. In accordance with the experimental findings, the existence of liquid filaments of finite length (F−) with negative Laplace pressure can be theoretically excluded.

The morphology diagram for rectangular grooves in Figure 7b basically contains three different morphologies: droplets (D) and liquid filaments with positive (F+) and negative (F−) Laplace pressure. In contrast to triangular grooves, where solely morphologies with a single meniscus are found, all wetting morphologies in rectangular grooves may as well be found in coexistence with liquid wedges (W) for contact angles of $\theta \leq 45°$.

In the asymptotic regime of large volume $V \gg w^3$, all liquid filaments (F+) are again metastable with respect to droplets (D).

The dashed line bounds the region of control parameter where filaments (F+) are found as metastable minima with respect to large contact angles. The solid line separates the regions where droplets or liquid filaments with negative mean curvature (F−) are global minima of the interfacial energy.

A number of peculiarities can be observed at smaller aspect ratios. While decreasing the contact angle, droplets (D) undergo a continuous transition to droplets in coexistence with filled wedges (W) at virtually zero Laplace pressure in sufficiently shallow grooves with $X \leq X_o \simeq 0.21$. Complete groove filling sets in when crossing the solid line at smaller contact angles. A transition from pinned wedges (pW) to unpinned "corner" wedges (cW) occurs for aspect ratios in the range between X_o and $X = 0.5$ as the contact angle is decreased to small values well below $\theta = 45°$.

Let us compare the interfacial free energy $f(\upsilon)$ according to eq 1 in grooves of rectangular and triangular cross sections at the "filling transition". In rectangular grooves with aspect ratios $X > X_o$ and contact angles $\theta < 45°$, a completely dewetted groove and a homogeneously filled groove exhibit the same interfacial free energy if the contact angle equals the filling angle

$$\theta_o = \arccos\left(\frac{1 - X^2}{1 + X^2}\right) \qquad (2)$$

as indicated by the solid line above 45° in Figure 7b.[13] The example in Figure 5b for $\theta = 54°$ demonstrates that, at the filling transition $\theta = \theta_o$ at zero pressure, all homogeneous liquid configurations with a volume smaller than the volume of the filled state are energetically less favorable than the filled and the completely dry state. In the case of triangular grooves (see Figure 4b for $\theta = 54°$), however, one finds a whole branch of homogeneous morphologies of the same interfacial free energy. In other words, there is no preferred position of the liquid−vapor interface in a triangular groove at the filling transition $\theta = \psi$, in sharp contrast to a rectangular groove, where we find an energy barrier that separates the dry state from the filled state.

The above discussion strongly suggests a comparison of the morphological transitions observed for the two groove geometries in a more systematic manner. To this end, we envisage the cross section of a groove as described by a function $y = h|2x/w|^\nu$. This may be represented in a scale-invariant way by a shape function $g(\tilde{x}) = 2X|\tilde{x}|^\nu$, where $\tilde{x} = 2x/w$. The rectangular groove then corresponds to the limit $\nu \rightarrow \infty$, whereas the triangular groove is described by $\nu = 1$ and $X = (1/2)\tan\psi$.[41] This enables a direct comparison of the two cases, as shown in Figure 8. Whereas the overall behavior is similar, note that while there is a kink in the solid curve representing the rectangular cross section but the corresponding curve for triangular channels is smooth. We will come back to this point later.

3.4. Electrowetting Experiments. When combined with a technique that provides direct control over the apparent contact angle, one may switch between different static wetting morphologies and induce net liquid transport along the grooves. An easy to use technique to vary the contact angle is the electrowetting effect[8,24−27] as we will describe briefly in the following text.

A conducting liquid is placed on a conducting substrate covered with a thin dielectric layer. When a voltage is applied between the droplet and the conducting substrate, the field energy stored in the resulting "capacitor" leads to an increase in its area, which is concomitant to a decrease in the apparent contact angle. This typical electrowetting setup on a dielectric (EWOD) is sketched in Figure 9a.

(41) Interestingly, the case of $\nu = 1/2$ and $h = w$ asymptotically yields the shape of two touching cylinders.

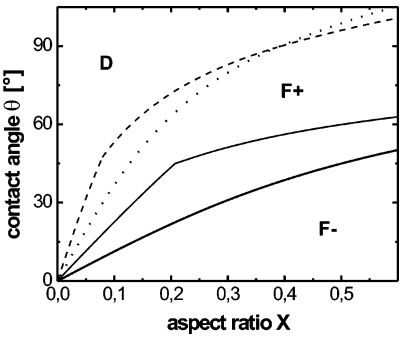

Figure 8. Direct comparison of the morphology diagrams for triangular ($\nu = 1$) and rectangular grooves ($\nu \rightarrow \infty$). Similar to Figure 7a, the dashed curves indicate the transition from droplets to filaments with positive Laplace pressure (---, rectangular grooves; ···, triangular grooves), and the solid curves indicate the transition from positive to negative Laplace pressure filaments (upper curve, rectangular grooves; lower curve, triangular grooves). For intermediate values of ν, one might expect boundaries intermediate to those displayed in the graph.

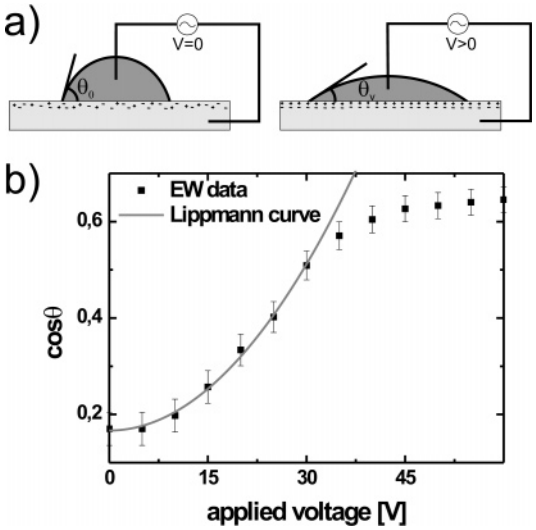

Figure 9. (a) Sketch of the electrowetting setup on a dielectric (EWOD). The droplet and the conducting Si substrate form a capacitor with the dielectric SiO_x layer. (b) Electrowetting curve for the system consisting of triangular grooves used in our experiments. For the used frequencies in the range of 1−30 kHz, no influence on the apparent contact angle was detectable.

The conducting liquid used for all electrowetting experiments presented here was a mixture of water, glycerol, and salt in a weight ratio of 17:80:3, which is hygroscopically stable against volume change under typical laboratory conditions.[22] The conductivity of this solution is $\sigma_{bulk} = (0.11 \pm 0.04)$ S/m as measured by an Ecoscan-Con5 conductometer. As a conducting substrate, we used grooved silicon substrates prepared as described above. To create a homogeneous dielectric layer, an oxide layer with a thickness of $d = (1.0 \pm 0.15)\ \mu$m was thermally grown into the silicon in the case of triangular grooves and $d = (1.15 \pm 0.15)\ \mu$m in case of rectangular grooves. Subsequently, the surface was hydrophobized by grafting a self-assembled monolayer of OTS molecules (octadecyltrichlorosilane) on top of the substrate, again following standard procedures.[34] To minimize electrochemical effects, we used ac voltage throughout our electrowetting experiments. The applied frequencies were in the range of $\omega = 1-30$ kHz.

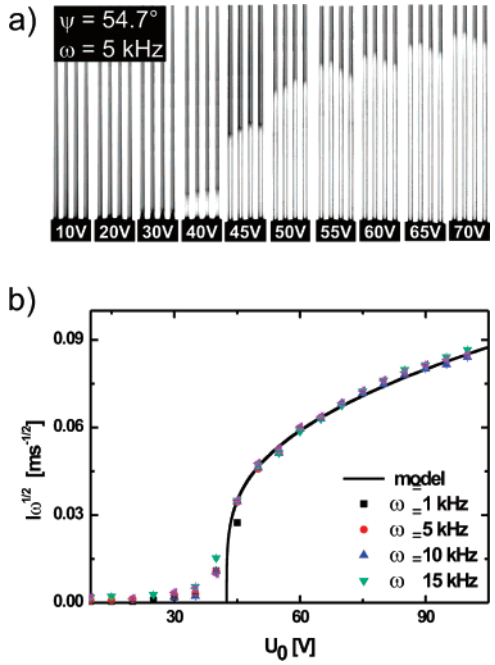

Figure 10. (a) Top view of a droplet advancing into grooves with a triangular cross section for different (equidistant) voltages. (b) Master curve for the length of the liquid filament as a function of the applied voltage for different frequencies. The solid line was obtained by numerically fitting eq 5 to the experimental data.

The typical dependence of the apparent contact angle on the applied voltage for the system used here is shown in Figure 9. The voltage is applied between a platinum electrode immersed in the droplet and the conducting silicon substrate. Up to about 35 V, the dependence of the apparent contact angle, θ_L, on the applied voltage, U, can be described by the so-called Lippmann equation:

$$\cos\theta_L = \cos\theta_Y + \left(\frac{U}{U_L}\right)^2 \qquad (3)$$

(See, for example refs 8, 24, and 27). The characteristic voltage is given by $U_L = \sqrt{2d\gamma_{lv}/\epsilon_0\epsilon_r}$, where ϵ_r is the dielectric constant of the silicon oxide layer and ϵ_0 is the dielectric permittivity of vacuum. With our experimental system, the apparent contact angle θ_L could be tuned from about 80° without any voltage applied, down to about 45° for an applied voltage of 100 V. The apparent contact angle is independent of the frequency ω of the applied voltage and the position on the wafer.

According to the predictions of the morphology diagram (Figure 7), liquid filaments can advance into triangular grooves from a large feeding drop upon decreasing the contact angle below the transition line between the morphologies (D) and (W) for decreasing contact angle. The series of optical micrographs in Figure 10a illustrates a typical groove-filling experiment on grooves with triangular cross sections and a wedge angle of $\psi = 54.7°$ at an applied ac voltage of $\omega = 5$ kHz. The experiment shows a clear threshold behavior for the groove filling, as expected from the theoretical consideration (Figure 7). A similar filament formation was explored for rectangular grooves[22,23] as shown in Figure 11a.

If the groove filling was solely governed by the relative capillary pressure between the feeding droplet and the filaments, then one would expect the filaments to grow indefinitely inside the grooves when the filling threshold is exceeded. However, the finite length is a direct result of the electrowetting effect, which is used to

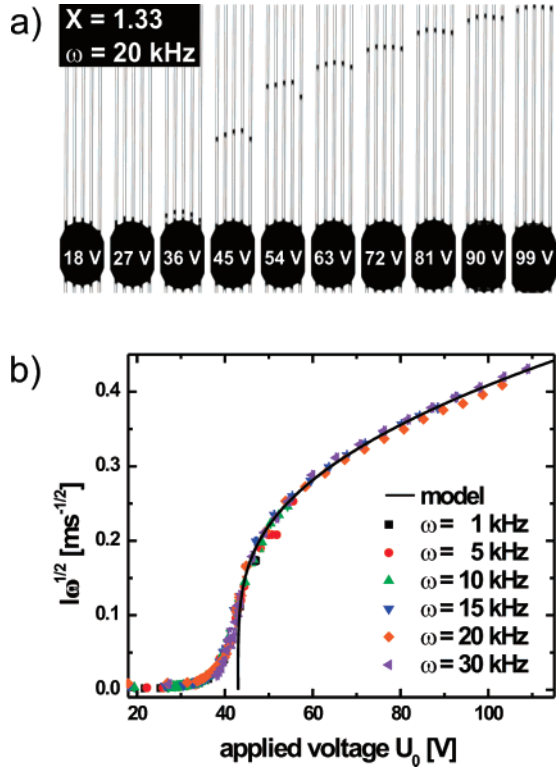

Figure 11. (a) Top view of a droplet advancing into grooves with a rectangular cross section for different (equidistant) voltages. The tips of the liquid filaments are black in the optical reflection micrographs. (b) Master curve for the length of the liquid filament as a function of the applied voltage for different frequencies. The solid line was obtained by numerically fitting eq 5 to the experimental data. For details, see ref 22.

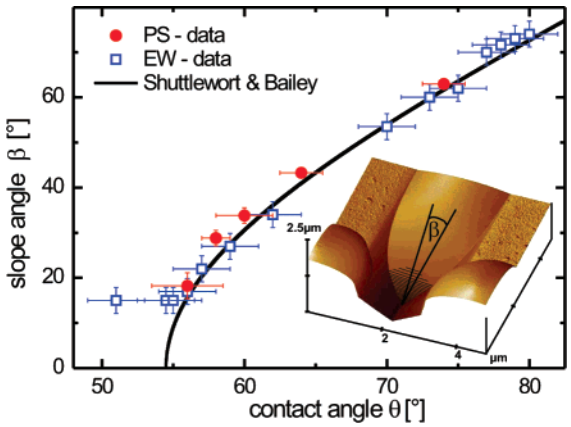

Figure 12. Slope angle β for different contact angles θ. Experimental points were obtained from experiments with polystyrene droplets and from electrowetting experiments (EW). The solid curve shows the expectation from Shuttlewort and Bailey[36] for a wedge angle of $\psi \simeq 54.7°$. (Inset) AFM micrograph showing the terminal part of the meniscus of a polystyrene droplet in a triangular groove.

vary the apparent contact angle. Because of the finite conductivity of the wetting liquid and the applied ac voltage, the voltage drops along the liquid filament, and with it the apparent contact angle increases along the liquid filament. The voltage at the tip of the filament equals the critical voltage for groove filling.[22] The voltage drop is faster the higher the frequency ω of the applied ac voltage, whereas the threshold voltage for groove filling is independent of the frequency (Figures 10b and 11b). Since a transmission line model has proven successful for rectangular grooves,[22] it may as well help us to understand the

length dependence of liquid filaments in triangular grooves on the amplitude and frequency of the applied ac voltage.

The liquid-filled groove is a conductive material of constant cross section surrounded by an insulating layer, which is electrically equivalent to a free-ended coaxial cable and can be described as a series of low passes along the direction of the grooves.[35] The voltage drops along an evenly filled groove with a characteristic decay length of

$$\lambda = \sqrt{\frac{4\pi d\sigma}{\omega\epsilon_0\epsilon_r}\frac{w\sin\psi}{4}} \tag{4}$$

The length λ is composed of two characteristic length scales of our system: an electrical length scale of $4\pi d\sigma/(\epsilon_0\epsilon_r\omega)$ representing the electrical properties of the material and a geometrical length scale that is the ratio of the area of the cross section divided by the wetted surface area, $w\sin(\psi/4)$. For grooves with a rectangular cross section, the geometric length scale has to be replaced by $wh(w + 2h)$.[22] An analytical expression between the applied voltage at the drop, U_0, and the length of the liquid filament, l, was derived in ref 22

$$U_0 = U_T\sqrt{\cosh^2\left(\frac{l}{\lambda}\right) - \sin^2\left(\frac{l}{\lambda}\right)} \tag{5}$$

where U_T is the threshold voltage for the groove filling.

If we rescale the measured length of the filament, l, with the frequency-dependent term of $\lambda \propto \sqrt{1/\omega}$, then all data for different frequencies collapse onto a single curve as shown in Figures 10b and 11b. Equation 5 is numerically fitted to the experimental data (solid lines in Figure 10b) using the experimentally determined geometries of the grooves, the threshold voltage, and the dielectric properties of the system as input parameters. The conductivity of the liquid is the only fitting parameter, and was determined to be $\sigma_{tri} = (0.023 \pm 0.002)$ S/m.

In contrast to the rectangular grooves, where we could achieve a decent quantitative agreement ($\sigma_{rect} = (0.15 \pm 0.05)$ S/m), we cannot reach a quantitative agreement between the conductivity derived from the fitting procedure and the value measured for bulk samples ($\sigma_{bulk} = (0.11 \pm 0.04)$ S/m). We will come back to this point in more detail when discussing the qualitative differences of the filling and draining behavior between triangular and rectangular grooves.

3.5. Filling of Triangular versus Rectangular Grooves. It was first noted by Shuttleworth and Bailey[36] that the tip of a liquid droplet in triangular grooves becomes more and more pointed as the contact angle θ reaches the critical filling angle ψ. In their analysis, they assumed that the terminal part of the meniscus asymptotically becomes a plane upon approaching the tip, and they used the slope angle β to characterize the tip shape (inset of Figure 12). By elementary geometry, they derived a relation

$$\cos\beta\cos\psi = \cos\theta \tag{6}$$

that holds in the range $\theta > \psi$.

Later, Concus and Finn proved that any minimal surface in an infinite wedge (i.e., a surface of zero mean curvature) forming a constant contact angle with the wedge walls has to be a plane.[14] Because the shape of the wedge bottom is scaling-invariant, one can argue that, by "zooming in", the tip of a surface of finite constant mean curvature can be asymptotically regarded as a minimal surface (e.g., with zero mean curvature) on small length scales. This implies, in particular, that the very tip of any equilibrium shape in a wedge will asymptotically become a plane and that the predictions of Shuttleworth and Bailey should hold.

The slope angle β at the tip of vapor-condensed polystyrene morphologies was measured directly by AFM in tapping mode. All experimental values from the polystyrene morphologies compare well with the predictions of Shuttleworth and Bailey.[36] Because of limitations in preparing substrate wettabilities by grafting the SAM layer (and subsequent plasma treatment as explained above), contact angles closer to the filling threshold were not accessible. From this gradual filling transition it is already obvious that the assumption of a constant cross section of a liquid filament made in our electrical model is not fulfilled for filaments in triangular grooves. The conductivity derived from fitting the electrical model to the experimental data assuming a constant cross section of the liquid filament underestimates the (bulk) conductivity of the liquid.

Having a close look at the filling experiments by electrowetting, which allows to vary the apparent contact angle continuously, we even find a deviation from the tip shape predicted by Shuttleworth and Bailey very close to the critical filling angle. To analyze the corresponding tip slope β for our electrowetting experiments, we introduced an angle ϕ that is half of the tip angle as measured from a projection into the plane of the substrate as a quantitative measure of the tip pointedness. According to Shuttleworth and Bailey,[36] the opening angle ϕ of the tip satisfies the relation $\tan\psi\tan\phi = \tan\beta$. The data from the electrowetting experiments agree well with the condensation experiments and satisfy the Shuttleworth prediction down to a slope angle of about 15° as shown by the open squares in Figure 12. But very close to the filling angle, the tip slope β deviates remarkably from the theory of Shuttleworth and Bailey. This escape from the analytical model might be due to the predicted,[37] and very recently experimentally verified[38] crossover from the apparent electrowetting contact angle according to the Lippmann equation to the mesoscopic contact angle close to the three-phase contact line. The length of this crossover region scales with the thickness of the insulating layer. The apparent electrowetting contact angle θ_L determines the wetting properties on a macroscopic scale, but as the dimensions of the liquid morphology reaches the order of the thickness of the dielectric layer, the influence of the mesoscopic contact angle on the liquid morphology should influence the emerging wetting morphology. Thus, whenever the filling height of the liquid wedge falls below the thickness of the insulating layer we expect a visible deviation from the simple assumption that the material contact angle can be simply replaced by the Lippmann angle. If we estimate the length of the filament tip required to determine an angle ϕ with our optical setup to 5 μm, then a tip angle of $\beta = 15°$ corresponds to a filament thickness below 0.8 μm above the substrate, which is slightly less than the thickness of the insulating layer. In other words, a tip slope of $\beta = 15°$ is the upper detection limit for the deviations from eq 6 due to electrowetting effects in our optical microscopy setup.

As a consequence of the particular tip shape, the filling of triangular grooves from a large feeding drop does not happen in an abrupt manner. By decreasing the contact angle θ below the filling angle ψ, one observes a gradual elongation of the liquid filament in the triangular groove involving pointed tips and a final divergence of the total length. This gradual lengthening of the filament is qualitatively different from the filling behavior in grooves with a rectangular cross section. In the latter case, the liquid suddenly advances into the grooves once the threshold contact angle θ_o according to eq 2 has been reached.[13,22] The differences are clearly visible in the high-resolution optical

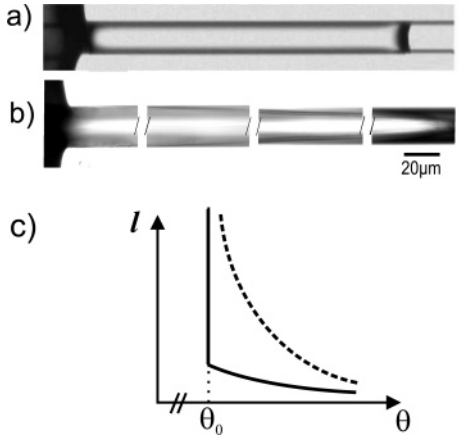

Figure 13. Optical micrographs of liquid filaments pulled out of large feeding droplets showing the homogeneous cross section in (a) a rectangular groove with an aspect ratio of $X = 1.33$ and (b) the continuously varying cross section in a triangular groove. (c) Schematic representation of the total length of the liquid filament, l, as a function of the contact angle, as found for rectangular (solid) and triangular (dashed) grooves.

micrographs (Figure 13a and b), showing a comparison between liquid filaments in rectangular grooves and in triangular grooves. For either geometry, the filaments have been drawn out by electrowetting.

This qualitative difference between the rectangular and triangular groove geometry at the filling transitions is in accord with observations made in the effectively 2D capillary model discussed above. The presence of an energy barrier between the dry and the filled state at the transition causes a finite crossover length between both states. Upon approaching the filling transition of a triangular groove, however, the energy barrier between the filled and the dry state vanishes at the filling transition. The corresponding divergence of the crossover length is responsible for nonhomogeneous morphologies with a slowly varying cross section that grows out of the feeding drop. Decisive features of this morphology are unpinned contact lines and a cross-sectional area that decreases with increasing distance from the feeding droplet. Hence, the electrical resistance of the liquid morphology in the groove increases with growing distance from the drop and explains the qualitative agreement between the simple electrical model in triangular grooves and the experimental groove filling data (cf., the solid lines in Figure 10b). If we consider the total length of the filament, l, which in the case of triangular grooves is identical to the crossover length, the qualitative difference between the two cases becomes particularly clear. In Figure 13 c, l is sketched qualitatively as a function of the contact angle, the latter with respect to the critical angle at which filling occurs, θ_c. However, in the case of triangular grooves (dashed curve), $l(\theta)$ is reminiscent of a continuous (or second-order transition), and it is discontinuous (or first order) in the case of rectangular grooves (solid line).

Going back to Figure 8, we find that the solid curve corresponding to the rectangular grooves represents a discontinuous transition. The lower solid curve corresponding to the triangular grooves, however, represents a continuous transition throughout. This shows that there is a wealth of additional structure in the range of $1 < \nu < \infty$, which is interesting to explore in detail. This will be left to future work.

The different filling behavior of triangular and rectangular grooves has remarkable implications for the electrowetting experiments. While the applied voltage is decreased, the terminal meniscus of an elongated liquid filament in a rectangular groove

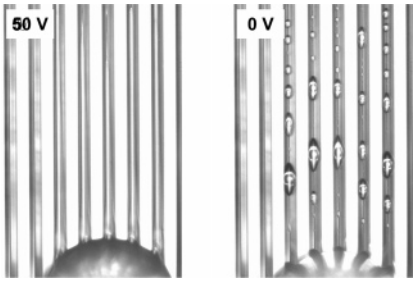

Figure 14. (Left) Top view of triangular grooves filled by means of electrowetting. (Right) Same sample after switching off the voltage. Dynamic instability of the liquid filament occurring when $\theta > \psi$ leads to the formation of isolated droplets.

retracts and is finally pushed back into the feeding droplet. Hence, filling and draining of grooves with rectangular cross sections are reversible and can be repeated many hundreds of times.[22,23] This is in strong contrast to the drainage behavior in triangular grooves. When the applied voltage is decreased, the liquid filament decays into a chain of isolated drops, as shown in Figure 14.

In the following text, we will give merely qualitative reasoning for this behavior: the three-phase contact line of the tilted liquid wedge is not pinned at the upper edges of the grooves and lies on a plane part of the substrate wall. After the voltage is switched off, the contact angle returns to a value above the filling threshold and a mechanically unstable wedge with positive mean curvature is formed. A local decrease in the filling height leads to a local increase in the Laplace pressure driving the liquid from regions with a smaller filling height to regions with a larger filling height. The initially linearly thinning liquid wedge transforms into droplets (D) or short filaments (F+). The typical periodicity of the pattern depends on the initial height of the liquid wedge and the difference between the apparent contact angle $\theta > \psi$ and the wedge angle of the groove ψ. This is discussed in detail in a separate publication.[28]

4. Conclusions

The comparison between equilibrium droplet shapes in contact with rectangular and triangular grooves demonstrates that the number of possible morphologies increases with the number of kinks and corners in the cross section of a groove. In both geometries, we find elongated structures and dropletlike morphologies. Their appearance is governed by the substrate wettabiliy and the aspect ratio of the grooves. In accordance with an analytical model based on 2D droplet shapes, we find liquid morphologies with a single meniscus and with two separate menisci in condensation experiments on rectangular grooves. Liquid morphologies on triangular grooves, in contrast, exhibit a single meniscus throughout.

In addition, we performed dynamic filling experiments using the electrowetting effect. Liquid is imbibed into grooves with rectangular and triangular cross sections once the contact angle reaches a certain critical value from above. The latter corresponds to the contact angle where liquid filaments of zero mean curvature are found in a groove of the respective geometry. At the filling transition, filaments with a constant cross section and with pinned contact lines advance into rectangular grooves. The length of the resulting liquid filaments can be quantitatively described with an electrical transmission line model[22] using the analogy of the filament consisting of a conducting liquid to a free-ended coaxial cable with finite conductivity. A similar threshold behavior is observed for the filling of triangular grooves. The shape of the advancing filament, however, is pointed, and its cross section is nonhomogeneous. The electrical model does not give satisfactory

quantitative results for triangular grooves, which can be explained by the varying cross section of the liquid. If the contact angle is switched back to a value above the threshold, these filaments decay into a chain of isolated droplets because the contact line of such a pointed filament is not pinned to the edge of the grooves.

The difference in the filling behavior can be explained from the 2D model that we put forward to explain the appearance of homogeneous and piecewise homogeneous liquid morphologies on linear surface topographies. The crossover length between the dry and the filled part of the groove is sensitively linked to the interfacial free energy as a function of the volume. In the case of rectangular grooves, we find an energetic barrier between the filled and the dry state that gives rise to a small crossover length. One may view the filling transition of the triangular grooves as being critical because the energy barrier vanishes at the transition, accompanied by a divergence of the crossover length. It will be interesting to investigate the order of the filling transition in grooves with a cross section of the scaling form $y = h|2x/w|^{\nu}$ with $\nu = 1...\infty$ by interpolating the triangular and rectangular cross sections as functions of the contact angle and aspect ratio.

Acknowledgment. The authors thank J. R. Henderson for bringing ref 36 to their attention. This work was supported by DFG priority program 1164 under grant number Se 1118/2. B.M.L. acknowledges support for this work through the U.S. National Science Foundation under grant number DMR-0603144.

LA701899U